PHYSICAL REVIEW E **89**, 050501(R) (2014)

Detection of an intermediate biaxial phase in the phase diagram of biaxial liquid crystals: Entropic sampling study

B. Kamala Latha,* Regina Jose, K. P. N. Murthy, and V. S. S. Sastry
School of Physics, University of Hyderabad, Hyderabad 500046, Andhra Pradesh, India
(Received 9 January 2014; revised manuscript received 16 April 2014; published 27 May 2014)

We investigate the phase sequence of biaxial liquid crystals, based on a general quadratic model Hamiltonian over the relevant parameter space, with a Monte Carlo simulation which constructs equilibrium ensembles of microstates, overcoming possible (free) energy barriers (combining entropic and frontier sampling techniques). The resulting phase diagram qualitatively differs from the universal phase diagram predicted earlier from mean-field theory (MFT), as well as the Monte Carlo simulations with the Metropolis algorithm. The direct isotropic-to-biaxial transition predicted by the MFT is replaced in certain regions of the space by the onset of an additional intermediate biaxial phase of very low order, leading to the sequence N_B-N_{B1}-I. This is due to inherent barriers to fluctuations of the components comprising the total energy, and may explain the difficulties in the experimental realization of these phases.

DOI: 10.1103/PhysRevE.89.050501 PACS number(s): 64.70.mf

The biaxial nematic phase of thermotropic liquid crystals, the existence of which was predicted quite early [1,2], has been receiving considerable attention recently, due to its expected technological advantage in display devices, in particular [3–5]. Though recent analytical treatments based on mean-field (MF) models [6–9] and Landau expansions [10–12], as well as computer simulations [13–18], support its feasibility, experimental success in polymeric systems, bent-core materials, and tetrapodes [19], on the other hand, has been relatively modest. Even then, interpretation and acceptance of some of these findings are still debated [20]. For example, an unsatisfactory aspect of the tetrapode system [21] is the low biaxial order observed, relative to the expectations (about 7%). The MF analysis, on the other hand, clearly identifies the regions of biaxial stability within the Hamiltonian parameter space, and predicts a universal phase diagram which includes a biaxial nematic phase with significant biaxial order [9]. The message from these studies is that the condensation of a biaxial phase under suitable experimental conditions should have been a rule, rather than an exception. The earlier Monte Carlo (MC) simulations, largely supporting the qualitative features of these theoretical predictions, were all carried out based on Boltzmann sampling. This procedure, however, has known limitations with systems possibly encountering free energy barriers. In this context, we report results obtained from a different sampling technique addressing such issues, indicating departures from the MF phase diagram.

Interactions among liquid crystal molecules with D_{2h} symmetry are described by a general quadratic Hamiltonian, expressed in terms of the orthogonal tensors associated with molecular axes ($\boldsymbol{e}$,$\boldsymbol{e}_\perp$,$\boldsymbol{m}$) as [9] $H = -U[\xi\, \boldsymbol{q}\cdot\boldsymbol{q}' + \gamma(\boldsymbol{q}\cdot\boldsymbol{b}' + \boldsymbol{q}'\cdot\boldsymbol{b}) + \lambda\, \boldsymbol{b}\cdot\boldsymbol{b}']$. Here, $\boldsymbol{q}$ is a symmetric, traceless and uniaxial tensor of the molecular major axis ($\boldsymbol{m}$) and $\boldsymbol{b}$ is a purely biaxial tensor expressed in terms of the other two molecular axes ($\boldsymbol{e}$ and $\boldsymbol{e}_\perp$), $\boldsymbol{q} = \boldsymbol{m}\otimes\boldsymbol{m} - \boldsymbol{I}/3$, $\boldsymbol{b} = \boldsymbol{e}\otimes\boldsymbol{e} - \boldsymbol{e}_\perp\otimes\boldsymbol{e}_\perp$. Setting the $\boldsymbol{q}$-$\boldsymbol{q}'$ coupling to be attractive ($\xi = 1$), the region of stability of the biaxial phase can be compacted to a triangular region in the (γ,λ) space, the so-called *essential triangle* (OIV in Fig. 1) [8]. All realizable systems of this Hamiltonian model can be mapped to a point within this triangle, based on symmetry arguments, by appropriate indexing of the molecular axes and by a suitable scaling of temperature. This interaction was studied in great detail within MF approximation ([8,9], and references therein), and a phase diagram was proposed [9] as a function of the arc length OIV, represented by λ^*, defined as $\lambda^* = \lambda$ on the segment OI, and $\lambda^* = (1+\sqrt{13}\gamma)/3$, with $\gamma = (1-3\lambda)/2$ covering the segment IV. The MF phase diagram predicts for $\lambda^* \lesssim 0.22$ ($\gamma = 0$, $\lambda \lesssim 0.22$) a two stage transition from the isotropic to a biaxial phase, with an intervening uniaxial nematic phase (resulting in the sequence of N_B-N_U-I). For the rest of the range of λ^*, a direct transition N_B-I is expected, extending up to V in Fig. 1. Predictions of the onset of a biaxial state in the asymptotic limit of reaching the point V (i.e., as $\lambda \to 0$) was noted to be unsatisfactory keeping in view the biaxial stability criteria [9].

In this context we carried out MC simulations of this model (employing a most commonly accepted cubic lattice of side $L = 20$, with periodic boundary conditions), based on an entropic sampling technique [22] employing the Wang-Landau algorithm [23] suitably modified for liquid crystal simulations [24] and augmented by frontier sampling [24,25]. This leads to the collection of an (entropic) ensemble of microstates distributed uniformly with energy, facilitated by prior computation of representative density of states of the system. Equilibrium ensembles at any desired (reduced) temperatures (T') are consequently extracted by a suitable reweighting procedure (RW ensembles) [26]. These encompass all permissible microstates consistent with the equilibrium conditions, overcoming inherent energy barriers, unlike their Boltzmann counterparts obtained by conventional Metropolis sampling [27] (B ensembles). We find that the phase diagram determined from the temperature variation of macroscopic averages of different observables (derived from the RW-ensembles) is in qualitative agreement with the MF predictions (and with the B-ensemble results) along the λ^* axis up to a point K (Fig. 1), beyond which present results deviate qualitatively from the MF predictions. Instead of a single N_B-I transition, we observe an additional biaxial-to-biaxial transition resulting in the sequence N_B-N_{B1}-I. The temperature of

*Corresponding author: kklata@gmail.com

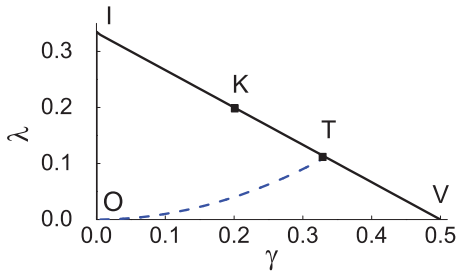

FIG. 1. (Color online) The essential triangle OIV, with arc length λ^* defined along the upper boundary. Points I,K,T,V are at $\lambda^*(\gamma,\lambda) \approx 0.33$ (0.0,0.333), 0.57 (0.197,0.202), 0.73 (1/3,1/9), and 0.93 (0.5,0.0), respectively. OT (blue dashed line) is the dispersion parabola ($\lambda = \gamma^2$) which intersects the side IV at T, the Landau point (LP).

the second transition decreases asymptotically to zero as the parameter λ^* tends to V (the limit of biaxial stability).

For the present discussion, the pairwise interaction is particularly transparent when expressed in terms of tensors appropriate to the symmetry of the diagonal IV (uniaxial torque along $\boldsymbol{e}$) as [9,28]

$$H = U'\left[\mu\left(\boldsymbol{e}\otimes\boldsymbol{e}-\frac{\boldsymbol{I}}{3}\right)\cdot\left(\boldsymbol{e}'\otimes\boldsymbol{e}'-\frac{\boldsymbol{I}}{3}\right) - (\boldsymbol{e}_\perp\otimes\boldsymbol{e}_\perp-\boldsymbol{m}\otimes\boldsymbol{m})\cdot(\boldsymbol{e}'_\perp\otimes\boldsymbol{e}'_\perp-\boldsymbol{m}'\otimes\boldsymbol{m}')\right], \quad (1)$$

where $U' = U(1-\lambda)/2$, $\mu = (1-9\lambda)/(1-\lambda)$. In this format, $\mu = -3$ corresponds to the point I (0,0.333) in Fig. 1, $\mu = 0$ to the Landau point T (1/3,1/9) (LP), and $\mu = +1$ to V (0.5,0.0). In particular, $\mu = -1$ corresponds to $\lambda^* \simeq 0.57$ (0.197,0.202) located at K.

RW ensembles are extracted at each λ^* value (from a total of 4×10^7 microstates distributed nearly uniformly covering the energy range of interest) at different temperatures with a resolution of 0.002 over the range (0.05–2.0). The computed averages include the energy per site (E) and the specific heat (C_v), the two relevant order parameters [uniaxial (R^2_{00}) and biaxial (R^2_{22}) orders [15,29], as well as their susceptibilities], and the Binder's energy cumulant V_4 [$= 1-\langle E^4\rangle/(3\langle E^2\rangle^2)$], which is a measure of the kurtosis [30].

We plotted the phase diagram obtained through this procedure, by choosing 56 values of λ^* distributed over the arc OIV (Fig. 1). Data exhibiting the onset of a second C_v peak for $\lambda^* \gtrsim 0.54$ (0.172,0.219), and thus differing qualitatively from the MF prediction, are plotted in Fig. 2. The location of the peaks of C_v profiles and of Binder's cumulant at different λ^* values, and identification of the liquid crystal phases from the corresponding order parameter variations (and their susceptibilities), result in the phase diagram shown in Fig. 3. The temperature T' of the simulation is scaled to conform to the values used in the mean-field treatment: $1/\beta^* = 3T'/(9[2U(1+3\lambda)])$ [9,31]. The MF and the current MC phase diagrams differ qualitatively beyond $\lambda^* \gtrsim 0.54$, very close to the point K ($\mu = -1$) (Fig. 1). Apart from the isotropic-to-biaxial transition at T_{C1}, the appearance of a second C_v peak at T_{C2} confirms a second biaxial-to-biaxial first-order transition mentioned above.

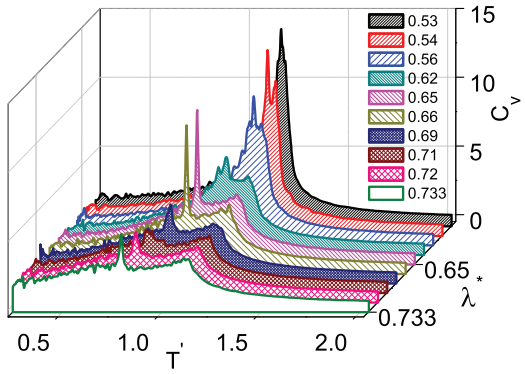

FIG. 2. (Color online) Specific heat C_v as a function of reduced temperature T' for various λ^* values in the range 0.53 (shaded black line) to 0.733 (unshaded green line) in the region KT of Fig. 1.

Specific heat profiles derived from the B and RW ensembles are depicted in Fig. 4(a), along with V_4 as an inset at $\lambda^* = 0.65$ (0.264,0.158). The corresponding order parameters, and their susceptibilities are shown in Fig. 4(b). The two order parameters exhibit a jump in their values coincident with the second low-temperature C_v peak. Specific heat derived from the B ensembles in contrast exhibits a broad hump below the high-temperature C_v peak [Fig. 4(a)]. It may be noted from Fig. 2 that this scenario persists at the Landau point also.

We depict the contours of the distribution of microstates in the entropic ensemble collected at LP plotted as a function of their energy and order parameters in Fig. 5. Superimposed on them are similar contour maps of microstates of B and RW ensembles equilibrated at the same temperature very close to T_{C2}. While the average values and widths of the energy distributions from the two canonical ensembles are seen to be comparable, distributions of the microstates with respect to the order parameters are very different. Relative to the B ensemble, the microstates belonging to the RW ensemble have different contour peak positions with larger fluctuations, with R^2_{00} visiting much higher values and R^2_{22} correspondingly much lower values. The observed differences in the thermal behavior of their respective averages are also shown [solid black line and dotted red lines in Figs. 5(a) and 5(b)].

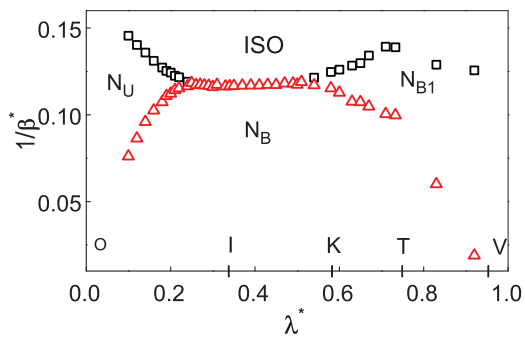

FIG. 3. (Color online) Phase diagram as a function of λ^* from RW ensembles. The transition temperature $1/\beta^*$ is scaled to conform to mean-field values as mentioned in the text. Specific points along OIV in Fig. 1 are indicated on the λ^* axis for reference. An additional biaxial-biaxial transition is observed in the region KTV in place of a single transition (to the biaxial phase) predicted by the mean-field theory.

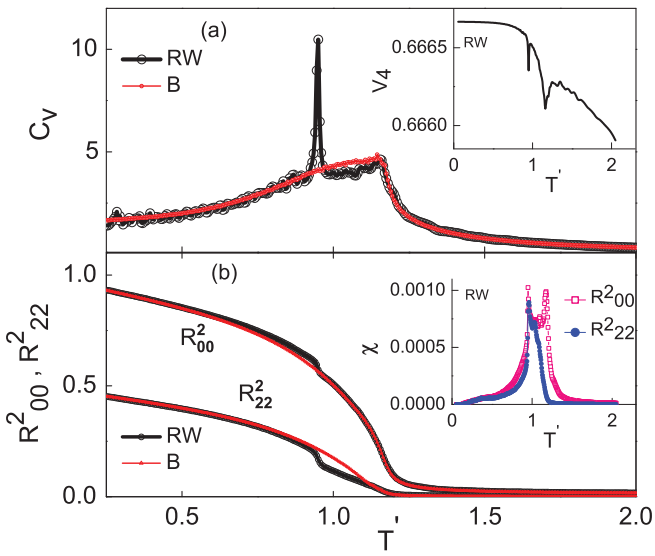

FIG. 4. (Color online) Temperature variation of (a) specific heat C_v (with energy cumulant V_4 as an inset), and (b) order parameters (with their susceptibilities as an inset), obtained from RW (thick black line) and B ensembles (thin red line) at $\lambda^* = 0.65$ (0.264,0.158). The susceptibility of R^2_{00} (empty squares) shows the signatures of both transitions, whereas the susceptibility of R^2_{22} (full circles) shows a single peak at T_{C2}. Clear signature of the second transition, and its first-order nature, may also be inferred from the V_4 data.

We examined the decomposition of the total energy of an approximate microcanonical ensemble into its components in the neighborhood of the second transition. For purposes of analysis, we now rewrite the Hamiltonian in terms of contributions from pairwise interactions between corresponding

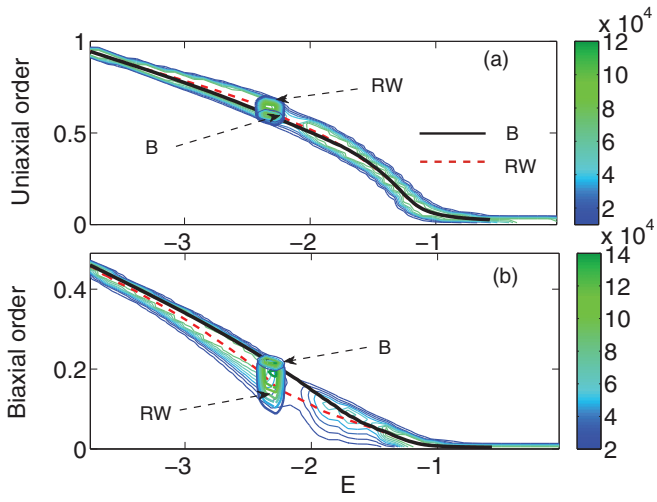

FIG. 5. (Color online) Contour plots of the distribution of microstates in the entropic ensemble at $\lambda^* \simeq 0.73$: (a) microstate energy versus its uniaxial order and (b) microstate energy versus its biaxial order. The contour maps of the distributions from RW and B ensembles equilibrated at temperature close to T_{C2} are superposed. The dotted red and thick black lines are the corresponding variations of thermal averages obtained from these ensembles, respectively.

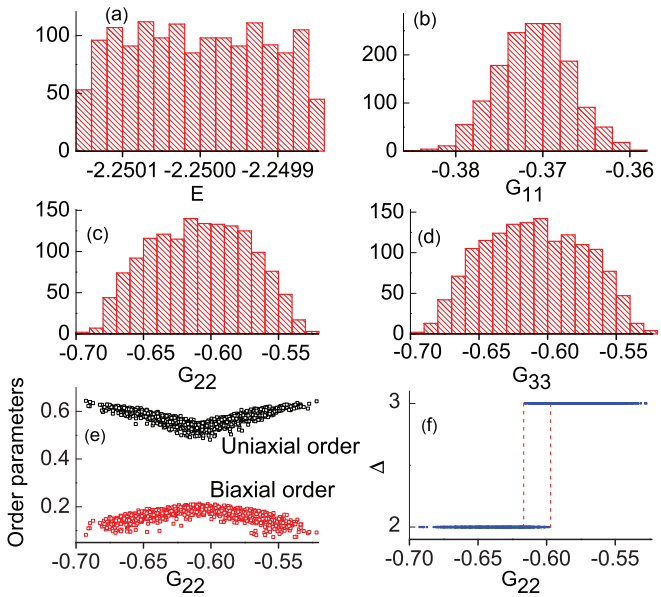

FIG. 6. (Color online) Microcanonical data at $\lambda^* = 0.65$ as a function of energy per site: (a) microstate energy distribution, (b) G_{11} distribution, (c) G_{22} distribution, (d) G_{33} distribution, (e) order parameters versus G_{22}, and (f) index of the eigenvector of maximum order of the microstates, Δ.

molecular axes [28], as

$$H = \epsilon[\mu G_{11} + (-2G_{33} - 2G_{22} + G_{11})]. \qquad (2)$$

Here, the indices $N = 1$, 2, and 3 represent the molecular axes $\boldsymbol{e}$,$\boldsymbol{e}_\perp$,$\boldsymbol{m}$, respectively, and $G_{jk} = P_2(f_{jk})$ where $P_2(\cdot)$ denotes the second Legendre polynomial. In a lattice model, f_{jk} represents the inner product of the jth axis of a molecule with the kth axis of a nearest neighboring molecule. We present our analysis of this ensemble in Figs. 6(a)–6(f). The distribution of the total energy (per site) of the microstates within a narrow range (-2.25 ± 0.0015) is shown in Fig. 6(a), while distributions of energy components $G_{11}(0.37 \pm 0.01)$, G_{22} (0.60 ± 0.07), and G_{33} (0.60 ± 0.07) are successively shown in Figs. 6(b)–6(d). Clearly the fluctuations of these components occur so as to conserve the total energy within its width. The interaction energies of the two molecular axes $\boldsymbol{e}_\perp$ and $\boldsymbol{m}$ with the corresponding axes of the neighboring molecules are seen to fluctuate more widely relative to the $\boldsymbol{e}$ axes coupling energies. Figure 6(e) shows the variation of uniaxial and biaxial order parameter values of the microstates with respect to G_{22} (similar plots result with respect to G_{33} as well). Interestingly, the fluctuations on either side of G_{22} about its average lead to an increase in the uniaxial order of the microstates, with simultaneous decrease in their biaxial order. This observation led to an examination of the ordering tensors $(\boldsymbol{Q}_{ee}, \boldsymbol{Q}_{\boldsymbol{e}_\perp\boldsymbol{e}_\perp}, \boldsymbol{Q}_{mm})$ of the three molecular axes, determining their respective maximum eigenvalues [15]. The eigenvector corresponding to the maximum of these maxima is then taken as the primary order direction (calamitic axis). Indexing its direction as Δ (Δ = 1, 2, and 3) for the three possibilities of the ordering tensors of $(\boldsymbol{e},\boldsymbol{e}_\perp,\boldsymbol{m})$ defining the calamitic axis of the sample, respectively, we show the variation of Δ with G_{22} in Fig. 6(f) (a complementary plot obtained with G_{33}). In a small

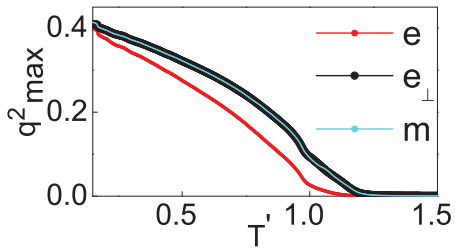

FIG. 7. (Color online) The long-range order of the three molecular axes ($\boldsymbol{e}$,$\boldsymbol{e}_\perp$,$\boldsymbol{m}$) at $\lambda^* = 0.65$, as a function of temperature. The order of the $\boldsymbol{e}$ axes (lower thin red line) shows a dramatic increase at T_{C2}.

central region of G_{22} (0.60 ± 0.01) a degeneracy of the top two eigenvalues (corresponding to the ordering tensors of the $\boldsymbol{e}_\perp$ and $\boldsymbol{m}$ axes) is observed, and hence the calamitic direction seems to fluctuate with equal probabilities within this narrow band between the corresponding eigenvectors (as an artifact of the inevitable rounding off errors during computation). For fluctuations outside this region, Fig. 6(f) shows that this degeneracy is lifted, and one of the eigenvectors (of tensors of $\boldsymbol{e}_\perp$ or $\boldsymbol{m}$) remains the unique calamitic axis depending on the sign of the fluctuation, indicating that the corresponding eigenvalue determines the dominant order, which is mapped to R^2_{00} by definition. The observed decrease of the biaxial order on both sides of the fluctuation [Fig. 6(e)] is a result of this circumstance. Further insight into the nature of the second transition could be gained by plotting the temperature variation of the long-range order of the three axes, represented by square of the maximum eigenvalues of the corresponding ordering tensors (Fig. 7). As expected on this diagonal, these values match for $\boldsymbol{e}_\perp$ and $\boldsymbol{m}$ axes, and progressively increase on cooling. The long-range order of the $\boldsymbol{e}$ axes, on the other hand, increases significantly only at the onset of the second low-temperature transition. It is this enhancement that seems to be promoting the onset of the second biaxial phase with observable macroscopic biaxiality.

In conclusion, we argue that, starting from the point K in Fig. 1, the initial biaxial phase condensing from the isotropic phase is the manifestation of the cooperative modes induced by the biaxial coupling of the $\boldsymbol{e}_\perp - \boldsymbol{m}$ axes [second term in Eq. (1)]. The subsequent biaxial-biaxial transition is mediated by the stabilizing effect of the long-range order of the molecular $\boldsymbol{e}$ axes [first term in Eq. (1)] brought into play at a lower temperature. In this context K $(\mu = -1)$ appears to be a unique point where the strength of the effective attractive coupling of the $\boldsymbol{e}$ axes becomes lower than the attractive biaxial coupling of the other two molecular axes, a phenomenon which continues as λ^* progresses on the diagonal. As the LP is reached, the former interaction progressively disappears, thereby pushing the corresponding transition temperature to lower values and weakening the first-order transition. The existence and description of the intermediate phase with no long-range order of the $\boldsymbol{e}$ axes seem naturally to be out of the valid regime of the MF theory. The absence of the signature of the second transition (Fig. 4) from the B ensembles and limited fluctuations of the order parameters [Figs. 5(a) and 5(b)], seem to be correlated. The observed trajectory in the configuration space derived from RW ensembles is qualitatively different beyond K and is not accessible to the standard Metropolis sampling due to the onset of barriers to the energy component fluctuations, originating from the lack of concomitant onset of long-range order of the three axes (inhomogeneity). The interesting discussions on antinematic interactions, covering the curious parameter region TV [28,32,33] provide complementary arguments as the Landau point is reached from the opposite side. We also find similar qualitative differences between RW and B ensembles in the interior of the triangle for large enough γ values (to be published). Finally, the existence of an in-principle intermediate biaxial phase of inherently low order (inhibited by inhomogeneities) seems to be a pointer to the difficulties in experimentally realizing a stable, macroscopic biaxial nematic phase.

We thank Professor N. V. Madhusudana (Raman Research Institute, Bangalore, India) for useful discussions. The simulations are carried out at the Centre for Modeling Simulation and Design, University of Hyderabad.

[1] M. J. Freiser, Phys. Rev. Lett. **24**, 1041 (1970).
[2] J. P. Straley, Phys. Rev. A **10**, 1881 (1974).
[3] J. H. Lee, T. K. Lim, W. T. Kim, and J. I. Jin, J. Appl. Phys. **101**, 034105 (2007).
[4] R. Berardi, L. Muccioli, S. Orlandi, M. Ricci, and C. Zannoni, J. Phys.: Condens. Matter. **20**, 463101 (2008).
[5] Mamatha Nagaraj, Y. P. Panarin, U. Manna, J. K. Vij, C. Keith, and C. Tschierske, Appl. Phys. Lett. **96**, 111106 (2010).
[6] A. M. Sonnet, E. G. Virga, and G. E. Durand, Phys. Rev. E **67**, 061701 (2003).
[7] G. De Matteis and E. G. Virga, Phys. Rev. E **71**, 061703 (2005).
[8] F. Bisi, E. G. Virga, E. C. Gartland Jr., G. De Matteis, A. M. Sonnet, and G. E. Durand, Phys. Rev. E **73**, 051709 (2006).
[9] G. De Matteis, F. Bisi, and E. G. Virga, Continuum Mech. Thermodyn. **19**, 1 (2007).
[10] A. E. Prostakov, E. S. Larin, and M. B. Stryukov, Crystallogr. Rep. **47**, 1041 (2002).
[11] David Allender and L. Longa, Phys. Rev. E **78**, 011704 (2008).
[12] G. De Matteis, Mol. Cryst. Liq. Cryst. **500**, 31 (2009).
[13] G. R. Luckhurst and S. Romano, Mol. Phys. **40**, 129 (1980).
[14] M. P. Allen, Liq. Cryst. **8**, 499 (1990).
[15] F. Biscarini, C. Chiccoli, P. Pasini, F. Semeria, and C. Zannoni, Phys. Rev. Lett. **75**, 1803 (1995).
[16] S. Romano, Physica A **337**, 505 (2004).
[17] G. De Matteis, S. Romano, and E. G. Virga, Phys. Rev. E **72**, 041706 (2005).
[18] G. Sai Preeti, K. P. N. Murthy, V. S. S. Sastry, C. Chiccoli, P. Pasini, R. Berardi, and C. Zannoni, Soft Matter **7**, 11483 (2011).
[19] K. Severing and K. Saalwachter, Phys. Rev. Lett. **92**, 125501 (2004); L. A. Madsen, T. J. Dingemans, M. Nakata, and E. T.

Samulski, *ibid.* **92**, 145505 (2004); B. R. Acharya, A. Primak, and S. Kumar, *ibid.* **92**, 145506 (2004); K. Merkel, A. Kocot, J. K. Vij, R. Korlacki, G. H. Mehl, and T. Meyer, *ibid.* **93**, 237801 (2004); J. L. Figueirinhas, C. Cruz, D. Filip, G. Feio, A. C. Ribeiro, Y. Frere, T. Meyer, and G. H. Mehl, *ibid.* **94**, 107802 (2005).

[20] K. Van Le, M. Mathews, M. Chambers, J. Harden, Quan Li, H. Takezoe, and A. Jakli, Phys. Rev. E **79**, 030701(R) (2009); N. Vaupotic, J. Szydlowska, M. Salamonczyk, A. Kovarova, J. Svoboda, M. Osipov, D. Pociecha, and E. Gorecka, *ibid.* **80**, 030701(R) (2009); T. Ostapenko, C. Zhang, S. N. Sprunt, A. Jakli, and J. T. Gleeson, *ibid.* **84**, 021705 (2011).

[21] F. Bisi, G. R. Luckhurst, and E. G. Virga, Phys. Rev. E **78**, 021710 (2008).

[22] J. Lee, Phys. Rev. Lett. **71**, 211 (1993); **71**, 2353 (1993).

[23] F. Wang and D. P. Landau, Phys. Rev. Lett. **86**, 2050 (2001); Phys. Rev. E **64**, 056101 (2001).

[24] D. Jayasri, V. S. S. Sastry, and K. P. N. Murthy, Phys. Rev. E **72**, 036702 (2005); D. Jayasri, Ph.D. thesis, University of Hyderabad, 2009 (LAP LAMBERT Academic Publishing, 2011).

[25] C. Zhou, T. C. Schulthess, S. Torbrugge, and D. P. Landau, Phys. Rev. Lett. **96**, 120201 (2006).

[26] R. H. Swendsen and J. S. Wang, Phys. Rev. Lett. **58**, 86 (1987).

[27] N. Metropolis, A. W. Rosenbluth, M. N. Rosenbluth, A. H. Teller, and E. Teller, J. Chem. Phys. **21**, 1087 (1953).

[28] G. De Matteis and S. Romano, Phys. Rev. E **78**, 021702 (2008).

[29] Robert J Low, Eur. J. Phys. **23**, 111 (2002).

[30] K. Binder, Z. Phys. B: Condens. Matter **43**, 119 (1981); Phys. Rev. Lett. **47**, 693 (1981).

[31] F. Bisi, S. Romano, and E. G. Virga, Phys. Rev. E **75**, 041705 (2007).

[32] G. De Matteis and S. Romano, Phys. Rev. E **80**, 031702 (2009).

[33] S. Romano and G. De Matteis, Phys. Rev. E **84**, 011703 (2011).